# LBL Assembled Laminates with Hierarchical Organization from Nano- to Microscale: High-Toughness Nanomaterials and Deformation Imaging

Paul Podsiadlo,[†] Ellen M. Arruda,[‡,¶] Eugene Kheng,[‡] Anthony M. Waas,[‡,⊥] Jungwoo Lee,[§] Kevin Critchley,[†] Ming Qin,[†] Eric Chuang,[†] Amit K. Kaushik,[‡] Hyoung-Sug Kim,[▽,○] Ying Qi,[∥,#] Si-Tae Noh,[▽,○] and Nicholas A. Kotov[†,§,∥,]*

[†]Departments of Chemical Engineering, [‡]Mechanical Engineering, [§]Biomedical Engineering, [∥]Materials Science and Engineering, [¶]Program in Macromolecular Science and Engineering, [⊥]Aerospace Engineering, [#]Electron Microbeam Analysis Laboratory, University of Michigan, Ann Arbor, Michigan 48109-2136, [▽]Department of Chemical Engineering, Hanyang University, Ansan 425-791, Kyounggi-Do, South Korea, and [○]R&D Center, Hepce Chem Company, Ltd., Ansan 425-836, Kyounggi-Do, South Korea

**ABSTRACT** Layer-by-layer assembly (LBL) can generate unique materials with high degrees of nanoscale organization and excellent mechanical, electrical, and optical properties. The typical nanometer scale thicknesses restrict their utility to thin films and coatings. Preparation of macroscale nanocomposites will indicate a paradigm change in the practice of LBL, materials manufacturing, and multiscale organization of nanocomponents. Such materials were made in this study *via* consolidation of individual LBL sheets from polyurethane. Substantial enhancement of mechanical properties after consolidation was observed. The resulting laminates are homogeneous, transparent, and highly ductile and display nearly 3× higher strength and toughness than their components. Hierarchically organized composites combining structural features from 1 to 1 000 000 nm at six different levels of dimensionality with a high degree of structural control at every level can be obtained. The functionality of the resulting fluorescent sandwiches of different colors makes possible mechanical deformation imaging with submicrometer resolution in real time and 3D capabilities.

*Address correspondence to kotov@umich.edu.

The layer-by-layer assembly (LBL) technique[1] is currently one of the most widely utilized methods for the preparation of multifunctional, nanostructured thin films with applications ranging from nanocomposites,[2−4] drug delivery platforms,[5] antireflection coatings,[6] solid-state memory devices,[7] and superhydrophobic coatings.[8,9] Its popularity stems from simplicity and universality, as well as robustness and versatility in combining a plethora of available colloids and macromolecules into finely tuned architectures with nanometer scale control.[10,11] While quite beneficial in some areas of technology, for instance sensing, electronic materials, and transport phenomena, the typical nano- to microscale thicknesses of the LBL sheets and coatings limit their application in technologies where mechanical loads exerted on the material are fairly high. This is an impeding factor, for instance, for the production of ultrastrong composites made by LBL of interest to a variety of industries.[2−4] Modified LBL methods that accelerate the composite accumulation process have been proposed, including spraying,[12] spin-coating,[13,14] and dewetting LBL;[15] however, all of these techniques have yet to demonstrate the ability to form macroscale structures. Another solution can be found in a recently developed mode of LBL, the so-called "exponential" LBL (e-LBL), which is based on "in-and-out" diffusion of polyelectrolytes, which, along with other techniques, is taken advantage of in the study presented here.[16]

In this work, we set the goal of demonstrating that (1) materials with macroscale thicknesses, suitable for different forms of manufacturing, can be produced by the LBL technique; (2) these materials exhibit unique mechanical and optical properties; and (3) the LBL method of materials manufacturing can greatly improve the properties of the starting materials. We also explore the ability to accomplish these tasks by engineering these materials as hierarchically organized structures. Multiscale hierarchy is one of the fundamental design principles found in nature.[17] Compounding different levels of organization and functional engineering from the nanoscale to the macroscale is taken advantage of in the production of materials with exceptional strength, stiffness, hardness, and tough-

ness.[17] Such materials are exemplified by seashell nacre,[18] teeth,[19] bones,[20] spider silk,[21] and squid beak,[22] which are being studied as model systems for development of advanced, high-performance composites. The challenge in utilization of hierarchical design and achieving similar mechanical and structural features in synthetic materials lies in the difficulty of robustly traversing different length scales and combining features at multiple levels.[17] Here we give a first example of hierarchical structures that can traverse materials organization from 1 to $10^6$ nm at six different levels of dimensionality by consolidating individual free-standing LBL films. Along with simplicity of preparation, the resulting materials display high-toughness and ductility substantially exceeding the properties of the original polymeric materials. Other methods besides the one presented below of materials engineering at multiple scales can be developed, and one should expect similarly remarkable performances. Interesting functional properties of the consolidated LBL films are demonstrated by combining films with different fluorescent colors for imaging of deformation in laminated structures with a high degree of spatial resolution.
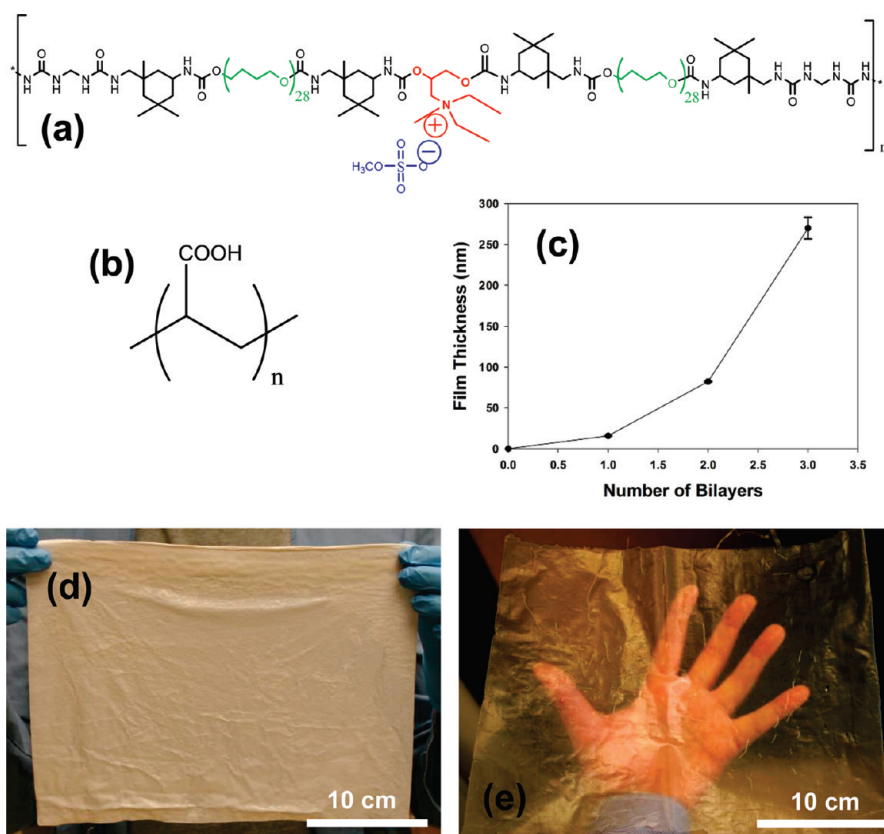


Figure 1. LBL assembly components, growth characterization, and free-standing LBL films. (a) Chemical structure of the cationic polyurethane copolymer. The cationic functional group of the polymer is highlighted in red, the counterion in blue, and the soft segments in green. (b) Chemical structure of poly(acrylic acid). (c) Ellipsometry results for film growth on top of polished silicon substrate showing rapid increase in thickness. Opaque appearance of the film prevented further measurements. Error bars for one and two bilayers are small and not visible in the graph due to difference in the magnitude of the values with the size of the y-axis. (d) Photograph of a 200-bilayer, hydrated PU/PAA free-standing sheet grown on 12 in. × 12 in. glass substrate. (e) Photograph of a 100-bilayer, dried PU/PAA free-standing sheet grown on the same 12 in. × 12 in. glass substrate as in (d).

## RESULTS AND DISCUSSION

Following the idea of hierarchical design, we started with the molecular level of organization and continued to the macroscale structure. One of the classes of materials well-known for their toughness is polyurethanes (PUs), which have found broad applications in construction, transportation, household appliances, packaging, electronics, and implantable biomedical devices, to name a few.

PUs have not previously been used in LBL assembly and, thus, represent an important new component of the LBL technique with a variety of potential research venues. For the purpose of this work, PU should be water-soluble and preferably charged. The chemical structure displayed in Figure 1a satisfies these requirements. This polymer has high solubility in water due to tertiary ammonium groups in the short side chains and a high density of hydrophilic groups along the backbone of the polymer. Note that it is probably one of the many possible charged PUs that can be synthesized, but this polymer was interesting to us, in particular,

because it has a fairly long "soft" segment $(-CH_2-CH_2-CH_2-CH_2-O-)_{28}$, imparting high ductility at the molecular and nanoscale levels.

LBL assembly of this PU was carried out by sequential dipping of a glass microscope slide for 30 s intervals into aqueous solutions of negatively charged poly(acrylic acid) (PAA, 1 wt %) and ~3.5 wt % PU (Figure 1a,b) using an automated dipping robot (see Experimental Details). The pattern of the multilayer accumulation showed clear evidence of e-LBL growth: ellipsometry showed a rapid exponential increase in the film thickness with additional bilayers (Figure 1c). The film was strongly hydrated, which is typical for e-LBL, and had a cotton-like appearance. Its opaqueness in this swollen state prevented us from performing ellipsometry studies beyond a few layers. However, cross-sectional scanning electron microscopy (SEM) clearly indicated successful continuation of growth of the films, revealing thicknesses of $10 \pm 3$ and $70 \pm 10$ μm for $(PU/PAA)_{18}$ and $(PU/PAA)_{100}$, respectively, where (PU/
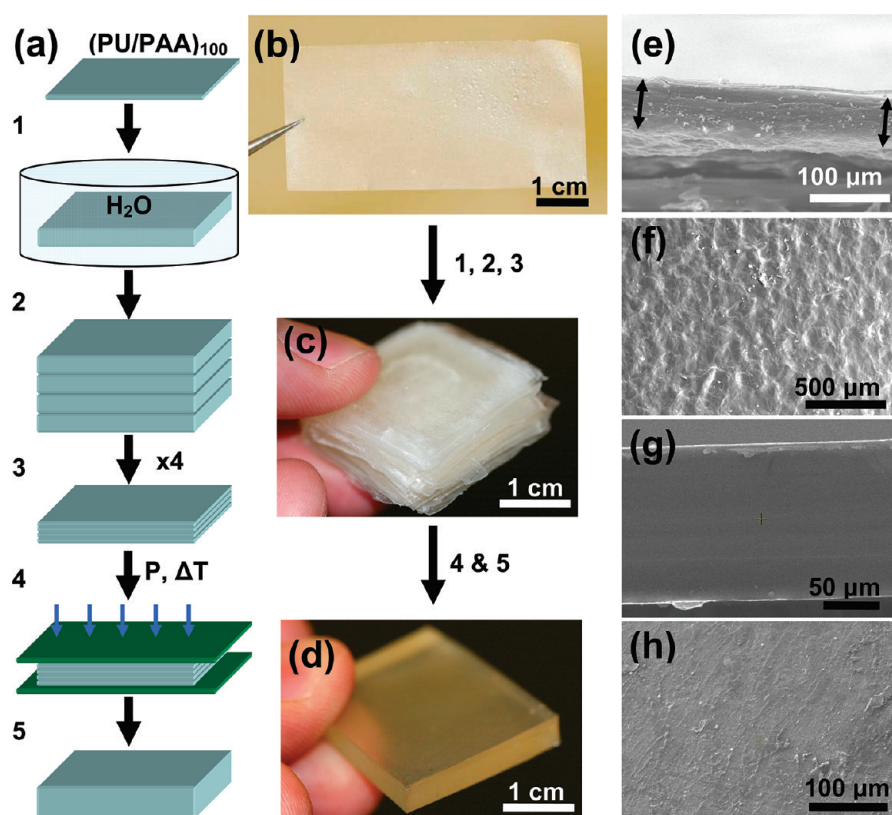
**Figure 2. Schematic of consolidation of free-standing e-LBL films. (a) Experimental procedure for consolidation of free-standing PU/PAA films: (1) the films are allowed to swell in water for ~1 h; (2) any number of films are stacked together into a sandwich structure to achieve conformal overlap; (3) the stack is dried at 100 °C under vacuum to remove any bubbles; (4) the dried stack is hot-pressed at 110 °C and <15 MPa of pressure; (5) final consolidated stack is removed from the press. (b) Photograph of a free-standing, 100-bilayer PU/PAA film before swelling. (c) Photograph of 100 × 100-bilayer, 1 in. × 1 in., free-standing films combined into a stack after swelling and drying. (d) Photograph of a final hot-pressed stack from (c). The total thickness of this stack is ~4.1 mm, and the total number of bilayers is 10 000. (e) SEM image of the cross section of a free-standing 100-bilayer PU/PAA film grown on a microscope glass slide. Arrows indicate the span of the cross section. (f) SEM image of the single 100-bilayer film in (e) revealing high surface roughness. (g) SEM image of the cross section of a consolidated sample composed of 5 × 100-bilayer PU/PAA films. The image shows complete coalescence of the interfaces between individual films. (h) SEM image of the top surface of the consolidated sample in (g).**
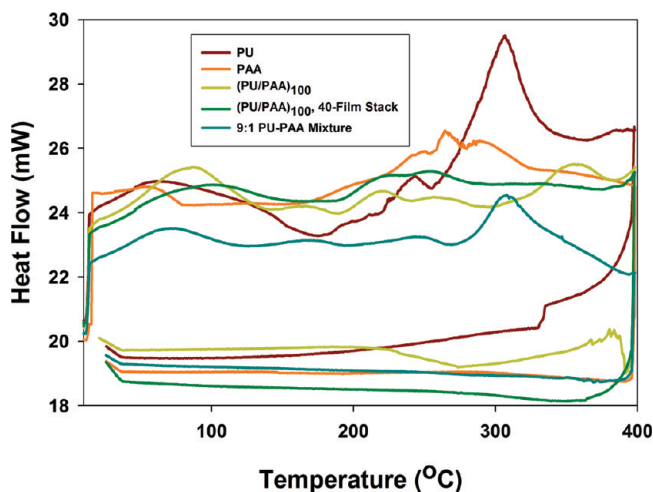
PAA)$_n$ represents the film obtained after $n$ deposition cycles.

Interestingly, although strongly swelling and hydrating, the films were easily separated from the substrate and handled (Figure 1d).[3] The free-standing films were found to be robust and strong, allowing for easy scale up to much larger substrates and film sizes (Figure 1d,e).

Continuing with hierarchical design of the materials and entering the micrometer/macroscale, we have exploited the swelling characteristic of the e-LBL films to combine together individual sheets into a laminated composite according to the schematic in Figure 2. In this simple strategy, dried films are first allowed to swell in water to increase their flexibility, and then they are overlaid on top of each other to achieve conformal overlap.

The swollen and hydrated interfaces interdigitate between adjacent films and promote consolidation of the stack into a homogeneous structure. The stack is further dried in order to remove water, and the structure compacts. Once dried, the stack is finally compressed under mild pressure, <15 MPa, and at a temperature of 110 °C. The applied pressure is necessary in order to provide intimate contact between individual sheets. We found that temperatures in the range of 110−120 °C are optimal for successful consolidation. Below 110 °C, there was no consolidation and films were easily peeled apart, and above 120 °C, the stacks showed signs of decomposition. Differential scanning calorimetry (DSC) analyses revealed that this temperature range corresponds to a broad peak which can be attributed to the crystalline melting point of the LBL composite (Figure 3).

Successful consolidation resulted in a homogeneous and transparent material. SEM characterization of the individual and consolidated structures revealed that the origin of the opaque appearance in single films is due to large surface roughness (Figure 2e,f). This roughness can be attributed to the non-uniform volume changes during drying of the swollen films and possibly other factors. In comparison, the consolidated samples showed uniform and homogeneous cross sections and surfaces, indicating that the hot-pressing procedure removes defects originating from LBL assembly.



**Figure 3. Differential scanning calorimetry analyses of PU, PAA, (PU/PAA)$_{100}$, (PU/PAA)$_{100}$ − 40-film stack, and PU/PAA blend. DSC trace of pure PU shows a broad peak at ~60 °C, a sharp shoulder peak at ~245 °C, and a sharp large peak at ~306 °C. Pure PAA also shows a broad peak ending at ~60 °C and a broad peak centered at ~265 °C.**

Investigation of mechanical properties indicated that the goals set forth in this work are realistic (Figure 4 and Table 1). Tensile mechanical properties of the base PU gave yield strength, $\sigma_Y = 4.3 \pm 0.5$ MPa; ultimate strength, $\sigma_{UTS} = 30 \pm 3$ MPa; Young's modulus, $E = 55 \pm 5$ MPa; and ultimate strain, $\varepsilon_{UTS} = 420 \pm 30\%$. The available literature data for PAA give $\sigma_{UTS} = \sim 4.5 - 12.3$ MPa and $\varepsilon_{UTS} = \sim 2 - 116\%$; they correspond to the hydrated state due to the highly hygroscopic nature of the polymer.[23,24] Compared to pure PU, in-plane tensile properties of single LBL films showed a 3× increase in $\sigma_Y$ to 12 MPa, no change in $\sigma_{UTS}$, and $\sim$4× improvement in $E \sim 230$ MPa. The ultimate strain of $\varepsilon_{UTS} \sim 250\%$ constitutes a reduction by nearly half in comparison to PU and a substantial improvement compared to PAA. This was an encouraging result since none of the previously reported LBL films[2−4,25−27] showed this level of ductility.

Tensile tests on consolidated samples showed marked improvement of the modulus ($E$ to $\sim$340 MPa) and dramatic improvements in both the strength ($\sigma_{UTS} \sim 85$ MPa) and the strain ($\varepsilon_{UTS} \sim 360\%$) over pure PU and single LBL films. The toughness of the composite stacks composed of 5- and 10-sheets was nearly $\sim$3× greater than that of pure PU.

The stacking-and-consolidation approach to preparation of materials is a simple and straightforward technique, which has been used before. Compared to previous studies of consolidation of plastic sheets,[28,29] there
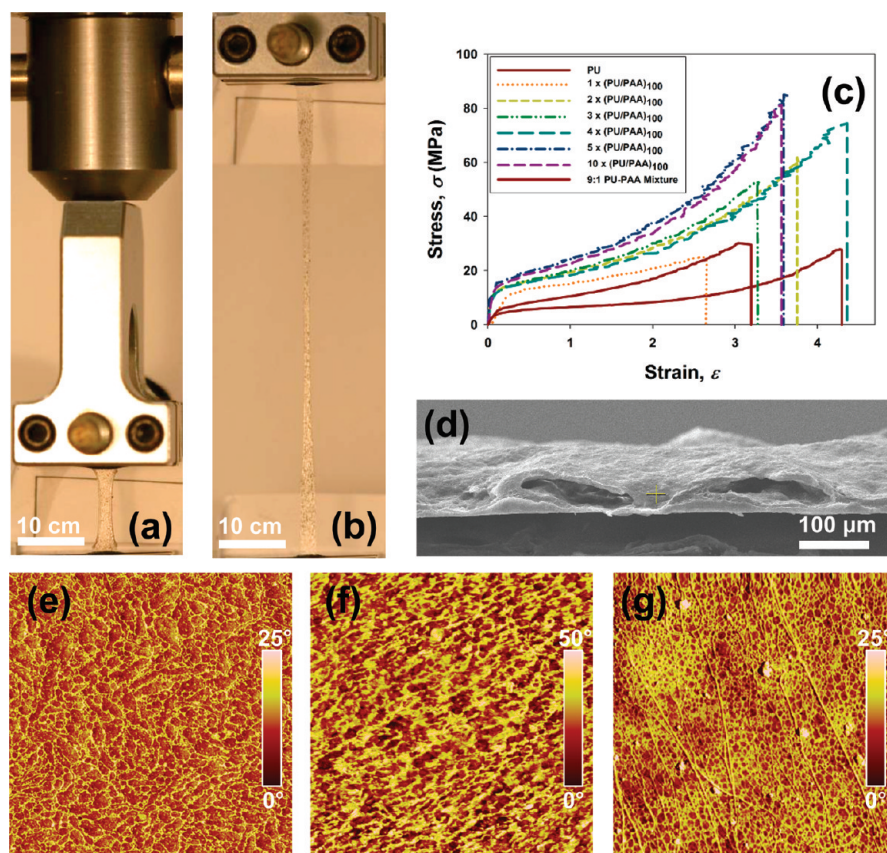


**Figure 4. Mechanical properties of PU/PAA e-LBL composites. (a) Photograph of a dog-bone specimen of a 10-film consolidated sample prior to tensile testing. (b) Photograph of the dog-bone specimen prior to rupture. Both images were taken at the same magnification and focal distance. The black dots on the surface of the specimens are paint marks which were used to accurately track the strain response. (c) Comparison of stress−strain responses for pure PU and consolidated samples composed of 1, 2, 3, 4, 5, and 10 films. (d) SEM image of the single, as-formed 100-bilayer film revealing pores in the interior of the film. (e−g) Phase-contrast atomic force microscopy (AFM) images of surface morphologies for PU, 9:1 PU/PAA mixture, and a five-sheet hot-pressed stack of e-LBL films, respectively. Each image represents a 5 μm × 5 μm area. Each sample was subjected to the same hot-pressing conditions.**

are several fundamental differences both in realization of approach and qualities of resulting materials when LBL films are used. First of all, the mechanical properties of the consolidated materials in traditional high-performance plastics were typically *lower* than those of

**TABLE 1. Summary of Mechanical Properties for PU, PAA, Single e-LBL Sheet, Consolidated PU/PAA e-LBL Structures, and a PU/PAA Blend in 9:1 Proportion by Weight**

| sample type | yield strength, $\sigma_Y$ (MPa) | ultimate tensile strength, $\sigma_{UTS}$ (MPa) | Young's modulus, $E$ (MPa) | ultimate tensile strain, $\varepsilon_{UTS}$ (%) | toughness, (MJ/m³) |
|---|---|---|---|---|---|
| PU | $4.3 \pm 0.5$ | $30 \pm 3$ | $55 \pm 5$ | $424 \pm 31$ | $49 \pm 6$ |
| PAA[a] | | $\sim 4.5 - 12.3$ | | $\sim 2 - 116$ | - |
| 1 Film | $12 \pm 1$ | $29 \pm 8$ | $228 \pm 135$ | $250 \pm 32$ | $48 \pm 14$ |
| 1 Film Hot-Pressed | $15 \pm 2$ | $29 \pm 7$ | $126 \pm 133$ | $172 \pm 55$ | $39 \pm 18$ |
| 2-Film Stack | $13 \pm 0.5$ | $54 \pm 18$ | $310 \pm 45$ | $366 \pm 74$ | $105 \pm 40$ |
| 3-Film Stack | $13 \pm 1$ | $53 \pm 5$ | $333 \pm 48$ | $344 \pm 46$ | $92 \pm 12$ |
| 4-Film Stack | $14 \pm 0.5$ | $61 \pm 13$ | $343 \pm 123$ | $362 \pm 65$ | $111 \pm 32$ |
| 5-Film Stack | $15 \pm 1$ | $86 \pm 4$ | $337 \pm 19$ | $361 \pm 10$ | $140 \pm 2$ |
| 10-Film Stack | $14 \pm 0.4$ | $85 \pm 3$ | $325 \pm 157$ | $356 \pm 10$ | $132 \pm 4$ |
| 9:1 PU/PAA Mixture | $6.4 \pm 0.3$ | $39 \pm 12$ | $58 \pm 6$ | $353 \pm 47$ | $66 \pm 23$ |

[a]Mechanical properties for PAA are taken from Nam *et al.*[23] and Huang *et al.*[24] Hot-pressing of individual LBL films does not lead to improvement of mechanical properties, although we cannot exclude the possibility that this observation depends on processing tools and actual press (see the Supporting Information).

the original macroscale sheets. In our case, we see that mechanical properties after consolidation are *higher* than those in the original sheets. Second, consolidation of sheets with controlled nanostructure was not carried out before. The importance of nanoscale organization for achieving desirable mechanical properties can be seen by comparison of a material prepared by simple blending of the components *versus* an LBL-structured PU/PAA composite (Table 1). The blended material gives inferior properties, even after consolidation.

Explanation of the marked improvement of mechanical properties from pure materials to LBL films and then to consolidated structures lies at combining structural features with different dimensionalities in the manner similar to biocomposites and biomaterials, which, in turn, control the deformation at different scales: molecular, nanoscale, and macroscale. At the molecular scale, the chemical composition of the LBL films was found by elemental analysis and X-ray photoelectron scattering spectroscopy (XPS) to be ~90 wt % PU and ~10 wt % PAA (see the Supporting Information). This large dominance of PU explains the high ductility of the composite. On the basis of the molecular weights of the repeat units, the ratio of the charged groups between PU and PAA is actually 1:9, which suggests that they form a complicated electrostatic and hydrogen-bonding network with one another. The XPS analyses also revealed the complete absence of sulfur (present in the sulfur-containing counterion, Figure 1a, blue color) in the LBL samples, which further suggests that all of the cationic groups directly interact with PAA *via* ionic and charge-dipole bonds. These cross-links, which are predominantly formed with the hard segments of the PU (Figure 1a, red and black groups), may give rise to improvements in strength and stiffness without significantly perturbing the elastic soft domains. FTIR analyses (Figure 5) further showed that hot-pressing of the films does not change the chemical signature of the material, that is, by formation of new bonds from covalent cross-linking, thus further supporting the idea of ionic cross-linking reinforcement. Our observation bears similarities with a recent work on selective reinforcement of hard domains in polyurethanes with clay nanosheets.[30]

Comparative characterization of a blend of the two polymers prepared by simple mixing is quite revealing about the role of nanoscale organization. The blend showed only a slight improvement of $E$ and $\sigma_{UTS}$ over pure PU. The comparison also demonstrated dramatic improvements of almost all mechanical properties in the e-LBL material *versus* the PU/PAA blend (Figure 4c and Table 1). This suggests that the nanostructuring imparted by the LBL deposition process may significantly alter the morphology of the composite. Indeed, atomic force microscopy (AFM) imaging of PU, PU/PAA blend, and PU/PAA e-LBL materials showed that they have dra-

matically different patterns and domain connectivity (Figure 4e−g). The nanoscale morphology in LBL films can be described as a cellular network of soft (bright) and hard (dark) molecular domains with the presence of linear domains oriented parallel to the dipping direction. The approximate size of domains in the blend obtained by simple solution mixing and drying of the components is 80−300 nm, while the cellular network domains in LBL films have approximate diameters of 150 nm with the elongated domains having widths of 30−50 nm and lengths as large as 5 μm and above. The difference in hardness contrast is also much greater in the blend than in the LBL film, suggesting that the multilayers are significantly more uniform. The pattern of domains in the LBL films has also some similarities with that of pure PU. The size of cells is substantially larger in PU, and there are no linear features. Difference in nanoscale organization also shows up in the DSC results (Figure 3). In comparison with both pure polymers and blended samples, which have similar DSC signatures, the LBL samples display either suppression or a shift to higher temperatures for all of the DSC peaks. This indicated much stronger interaction between the polymers in LBL materials. Wide-angle X-ray scattering (WAXS) results indicate there is no difference in crystallinity in LBL *versus* blended samples (Figure 6).

At the macroscale, hierarchical structuring in the lamination process also provides an important mechanism for property improvement related to defect mitigation. Every film has some number of defects, and in free-standing LBL films, they can be seen in the non-uniform thickness in Figures 2e,f and in apparent pores in the cross section (Figure 4d). Consolidation of the films gradually removes the defects with increasing thickness of the stack by (a) compressing the pores into continuous, solid material; (b) partial melting of the material and healing of the defects; and (c) cooperative sealing of the surface defects by adjacent films.

It is instructive to analyze the degree of structural control of hierarchical systems in the previously reported cases of hierarchically organized materials and the case of consolidated LBL films from PUs. The most typical hierarchical materials involve structural features at the scales of $10^0$ and $10^2$ nm.[31−36] Only two studies among many indicate hierarchy in respect to more than two scales.[37,38] Importantly, the range of variations within each level of hierarchy is typically quite limited also. Applying the same metrics, the method of manufacturing of hierarchical material described in this work allows the hierarchical organization at the scales of $10^0$ nm—the molecular structure of polyurethanes and the lower limit of the thickness of individual LBL bilayers deposited in one cycle (Figure 1); $10^1$ nm—the typical dimensions of hard domains in polyurethanes; $10^2$ nm—phase separation patterns in polymer blends (Figure 4); $10^2−10^5$ nm—individual free-standing LBL films in (Figure 2); $10^5−10^6$ nm—consolidated structures
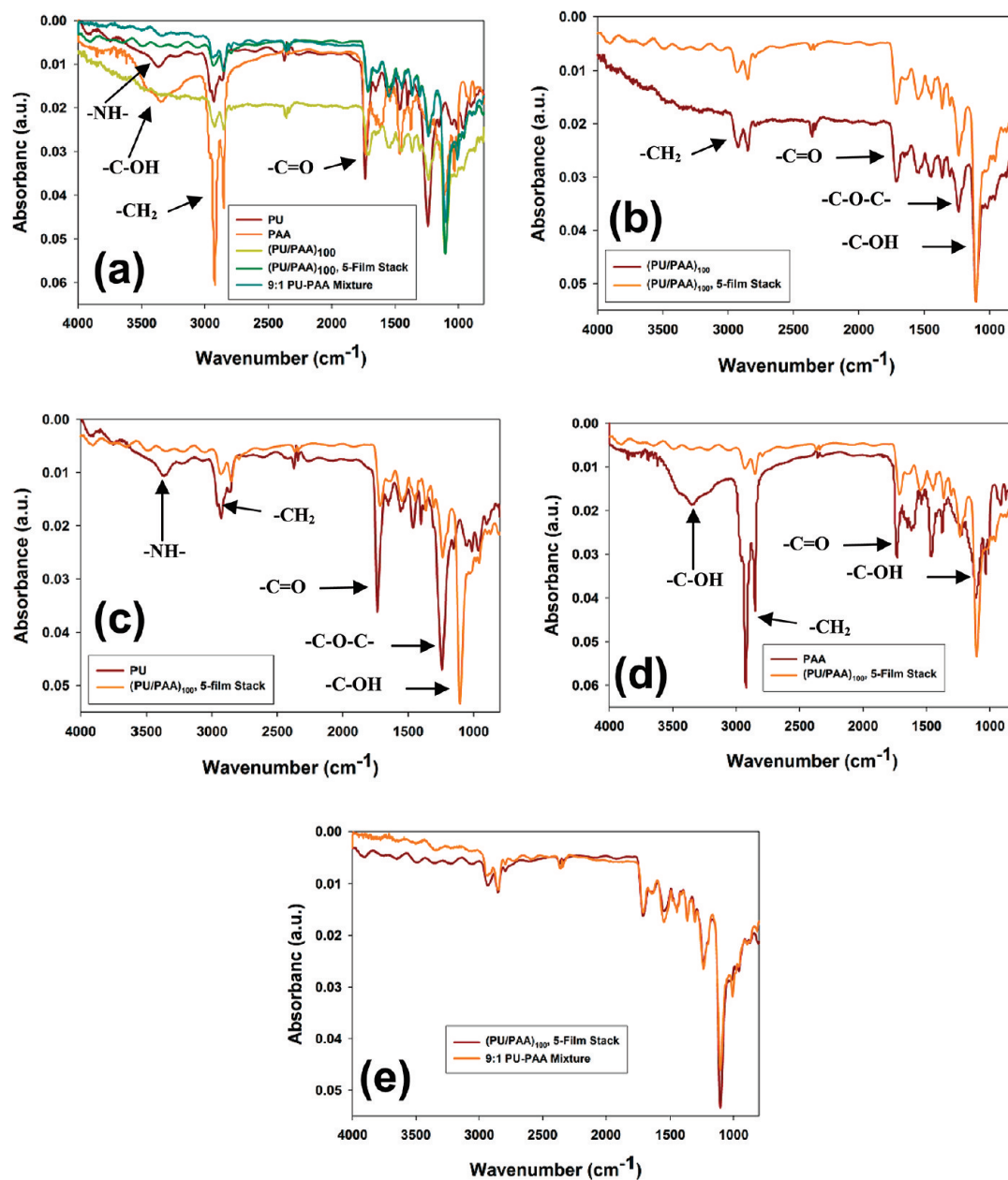
**Figure 5. FTIR comparison of chemical composition and hot-pressing effect on chemical composition of PU/PAA e-LBL films.
(a) Comparison of all materials. (b) Comparison of a single sheet and a five-sheet stack. (c) Comparison of PU and a five-sheet stack. (d) Comparison of PAA and a five-sheet stack. (e) Comparison of a five-sheet stack and a 9:1 PU/PA mixture. Some peak assignment can be made as indicated in the images: (PU) −NH− peak at ~3370 cm$^{-1}$, alkyl double peak at ~2930 cm$^{-1}$, a −C=O− peak of urethane at ~1740 cm$^{-1}$, and a −C−O−C− peak at ~1240 cm$^{-1}$; weak (PAA) −OH peak at ~3320 cm$^{-1}$ from hydrogen bonding and possible presence of water, and 2850 cm$^{-1}$, a −C=O− peak of carboxylic acid group at ~1740 cm$^{-1}$, and a −C−O− stretch at 1230 from a −C−OH group.**

available for further processing (Figure 7). Importantly, the variability of the size of hierarchical elements can be changed in a fairly wide range at every level of hierarchy without drastically alternating the hierarchical patterns and often overlap with dimensionality of the adjacent organizational levels. As such, the length of the soft and hard blocks in polyurethanes can be increased by about 1 order of magnitude. The same refers to the thickness of individual LBL film bilayers and free-standing films.

Besides mechanical property enhancement and the advent of a new approach to hierarchical materials engineering, the combination of LBL and stacking also offers opportunities for incorporation of useful optical properties in the resulting structures, which can also demonstrate the practical utility of such laminates. Thus, we prepared films with the addition of FITC and TRITC fluorescent dyes (Figure 7a). The dye-labeled films were sandwiched in different sequences and characterized using laser-scanning confocal microscopy. Al-
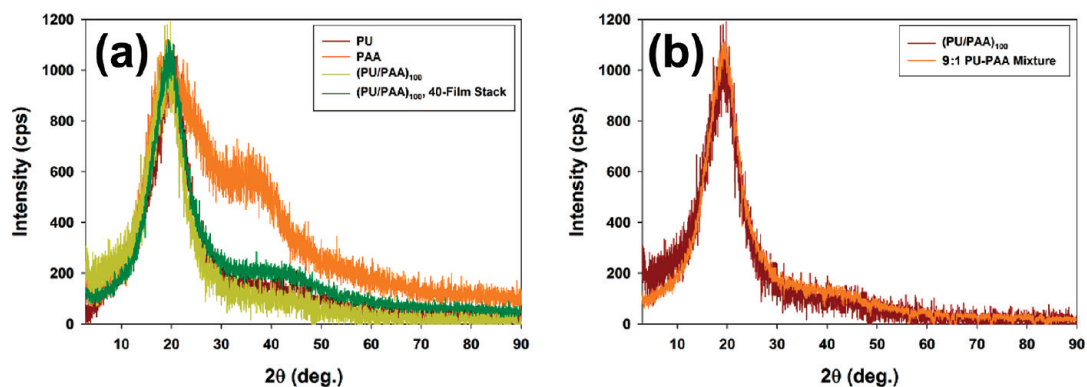
Figure 6. Comparison of WAXS spectra for (a) all the materials and (b) free-standing 100-bilayer (PU/PAA) LBL sheet and a 9:1 PU/PAA blend.

ternate stacking of green and red fluorescent films revealed that in spite of partial surface melting the films do retain their individuality (Figure 7b). This property can be used to manufacture multifunctional materials with a variety of applications because the films can equally well incorporate other molecules or nanoma-

terials besides the fluorescent dyes by their incorporation into the deposition sequence.[39]

A ∼1.2 mm thick sample in which the labeled films have been separated by three plain films was impaled with a small steel ball, and the resulting damage was imaged using confocal microscopy (Figure 7c). The abil-
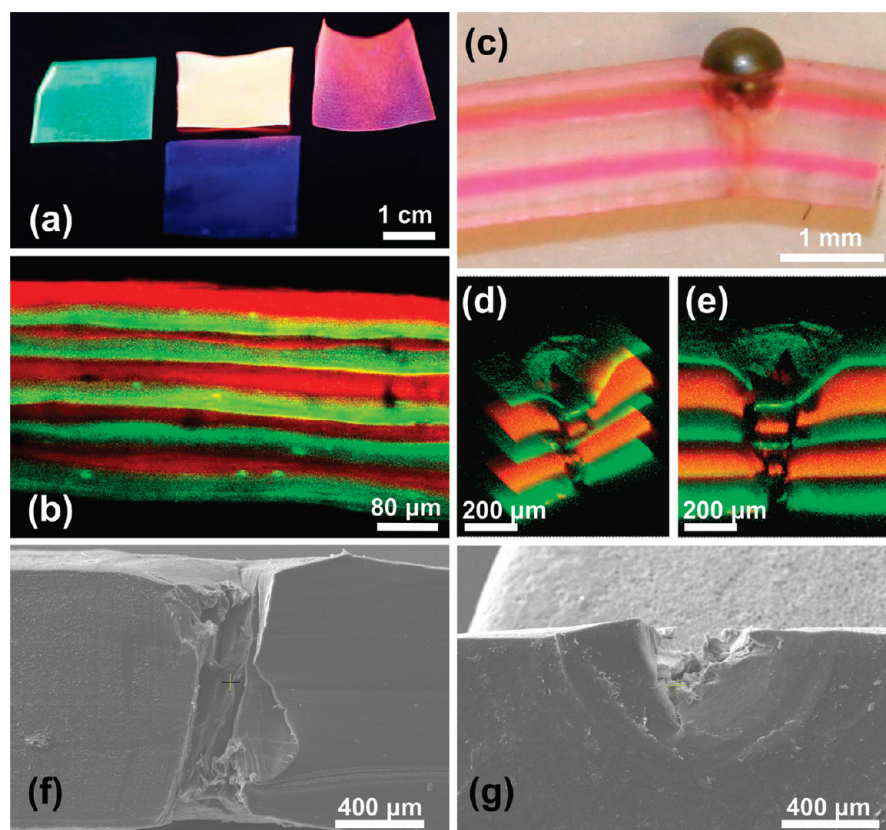


Figure 7. Demonstration of the multifunctional potential of the consolidated e-LBL structures. (a) Photograph of fluorescent-dye-labeled, 100-bilayer PU/PAA e-LBL films, and a consolidated stack under UV light (365 nm) illumination. Top row: (left) FITC-labeled 100-bilayer film, (center) consolidated stack composed of 10, 100-bilayer dye-labeled films, and (right) TRITC-labeled 100-bilayer film. Bottom: plain 100-bilayer film. The composite was prepared by alternate stacking of the dye-labeled films into a (FITC−/TRITC−)$_5$ structure. (b) Laser-scanning confocal microscopy image of a cross section of the dye-labeled 10-film alternating stack from (a). (c) Photograph of a cross section of a consolidated stack composed of alternating layers of FITC- and TRITC-labeled 100-bilayer films separated at every point by three, not-labeled 100-bilayer films. For demonstration purposes, a steel ball has been pressed into the film using a hydraulic press. The TRITC-labeled films are clearly visible as red bands. (d,e) Confocal microscopy 3D images of a cross section around the damage caused by the steel ball in (c). (f) Cross section SEM image of the damaged area from steel ball in (c). (g) Top-down SEM image of the damage caused by the steel ball.

ity of confocal microscopy to generate images of slices through the depth of the specimen at different focal lengths allows the user to generate 3D fluorescence images by stacking the individual slices in sequence. Using this feature, we were able to see the resulting damage in 3D (Figure 7d,e). Applying this technique in this context allowed us to visualize the structural deformations at different depths of the material, which would not be possible using optical or electron microscopes (Figure 7f,g). The confocal microscopy imaging offers a noninvasive damage detection method with excellent spatial resolution (~500 nm and smaller) when compared to other widely utilized techniques. Of the different methods available (*e.g.*, electrical conductivity, optical fiber detection, or ultrasonic evaluation), only high-resolution X-ray computed tomography (CT) has the capability of approaching a resolution of ~5 μm.[40] Better resolution is critical in understanding of deformation processes in advanced materials.

## EXPERIMENTAL DETAILS

**Materials, LBL Assembly, and Consolidation.** Cationic polyurethane aqueous dispersion (PU, ~35 wt %, MW ≈ 92 000) (Hepce Chem Co., South Korea) and poly(acrylic acid) (PAA, 35 wt %, MW = 250 000, pH = 2.9) were used as-received by diluting to ~3.5 and 1 wt % solutions, respectively, in deionized water. Fluorescein isothiocyanate isomer I (FITC) and tetramethyl rhodamine isothiocyanate (TRITC) fluorescent dyes were obtained from Sigma-Aldrich. PU/PAA multilayer films were prepared by conventional dipping LBL method using Midas II programmable slide stainers (EMD Chemicals. Inc.). In a typical assembly, 100-bilayer films of PU/PAA were prepared on microscope glass slides using 30 s dips in each of the solutions and 1 min rinses with water between each dipping. Free-standing films were isolated by etching of the glass slides with 1% hydrofluoric acid. After thorough rinsing with pure water, the films were dried in an oven at 100 °C. Laminated samples were prepared by hot-pressing overlaid stacks of films at 100 °C and <15 MPa of pressure for at least 30 min, depending on stack thickness. The blended sample was prepared by mixing the two components in a 9:1 wt % ratio, dry-casting, and hot-pressing using the same conditions.

**Mechanical Properties Evaluation.** The films were subjected to uniaxial tensile tests using a vertical tensile testing machine from Test Resources. Dog-bone-shaped test specimens were lightly airbrushed with a random, black speckle pattern before being cut with an elliptical punch to a gauge length of 13 mm and a width of 2−3 mm. The specimens were pulled apart at a displacement rate of 80 μm/s, and images of the center gauge section were collected every 5 s, using a Nikon D2x camera equipped with a 300 mm macrolens. The reactive tensile load on the specimen was measured using a 111 N load cell. The collected speckle images were analyzed using ImageJ software equipped with a MetaJ tracking macro. The $X$ and $Y$ coordinate data of two neighboring speckles as a function of specimen load were then processed with a MATLAB script to produce Green−Lagrange strain data corresponding to each load state. The Green−Lagrange strain $E_{11}$ in the direction of the axial force is defined as $E_{11} = 1/2[(1 + e_1)^2 - 1]$, where $e_1 = (dx - dX)/(dX)$ is the change in length per unit length of a line element that is parallel to the direction of axial stretching.[29] The force measurements from the load cell were divided by the measured initial thickness and initial width of the sample gauge section to give engineering stress. This procedure results in a plot of engineering stress *versus* $e_1$. Three to five samples were tested for each stack.

**Film-Structure Characterization.** SEM images were obtained with an FEI Nova Nanolab dual-beam FIB and scanning electron microscope operated at 15 kV beam voltage. Ellipsometry measurements were obtained using a BASE-160 spectroscopic ellipsometer produced by J. A. Woollam Co., Inc. The instrument was calibrated to the standard silicon wafer with a thin layer of silicon dioxide, and the subsequent calculations were fitted using a Cauchy model. Fluorescent images were obtained with Leica SP2 confocal microscope. IR spectra were obtained using a Nicolet 6700 spectrometer utilizing the grazing angle accessory (Smart SAGA) at a grazing angle of 85°. XPS was carried out using a Kratos Axis Ultra. A monochromated Al Kα X-ray source was used to irradiate the sample using a power of 140 W (14 kV, 10 mA). Elemental analysis was performed using a Perkin-Elmer 2400 Series II combustion analyzer. AFM experiments were performed in tapping mode using NanoScope IIIa instrument from Veeco Instruments (Santa Barbara, CA). X-ray powder diffraction (XRD) patterns were collected on a Rigaku Miniflex (Rigaku, The Woodlands, TX). The diffractometer is equipped with a Cu X-ray tube (Cu Kα, λ = 1.54059 Å) with an operating voltage of 30 kV and current of 15 mA. Scans were performed continuously from 2 to 90° 2θ in increments of 5° per min.

*Supporting Information Available:* Elemental and XPS analyses of the chemical composition in the composites. This material is available free of charge *via* the Internet at http://pubs.acs.org.

## REFERENCES AND NOTES

1. Decher, G. Fuzzy Nanoassemblies: Toward Layered Polymeric Multicomposites. *Science* **1997**, *277*, 1232–1237.
2. Mamedov, A. A.; Kotov, N. A.; Prato, M.; Guldi, D. M.; Wicksted, J. P.; Hirsch, A. Molecular Design of Strong Single-Wall Carbon Nanotube/Polyelectrolyte Multilayer Composites. *Nat. Mater.* **2002**, *1*, 190–194.
3. Tang, Z.; Kotov, N. A.; Magonov, S.; Ozturk, B. Nanostructured Artificial Nacre. *Nat. Mater.* **2003**, *2*, 413–418.
4. Podsiadlo, P.; Kaushik, A. K.; Arruda, E. M.; Waas, A. M.; Shim, B. S.; Xu, J.; Nandivada, H.; Pumplin, B. G.; Lahann, J.; Ramamoorthy, A. Ultrastrong and Stiff Layered Polymer Nanocomposites. *Science* **2007**, *318*, 80–83.
5. Wood, K. C.; Chuang, H. F.; Batten, R. D.; Lynn, D. M.; Hammond, P. T. Controlling Interlayer Diffusion to Achieve Sustained, Multiagent Delivery from Layer-by-Layer Thin Films. *Proc. Natl. Acad. Sci. U.S.A.* **2006**, *103*, 10207–10212.
6. Hiller, J.; Mendelsohn, J. D.; Rubner, M. F. Reversibly Erasable Nanoporous Anti-Reflection Coatings from Polyelectrolyte Multilayers. *Nat. Mater.* **2002**, *1*, 59–63.
7. Lee, J. S.; Cho, J.; Lee, C.; Kim, I.; Park, J.; Kim, Y. M.; Shin, H.; Lee, J.; Caruso, F. Layer-by-Layer Assembled Charge-Trap Memory Devices with Adjustable Electronic Properties. *Nat. Nanotechnol.* **2007**, *2*, 790–795.
8. Zhai, L.; Berg, M. C.; Cebeci, F. C.; Kim, Y.; Milwid, J. M.; Rubner, M. F.; Cohen, R. E. Patterned Superhydrophobic Surfaces: Toward a Synthetic Mimic of the Namib Desert Beetle. *Nano Lett.* **2006**, *6*, 1213–1217.
9. Zhai, L.; Cebeci, F. C.; Cohen, R. E.; Rubner, M. F. Stable Superhydrophobic Coatings from Polyelectrolyte Multilayers. *Nano Lett.* **2004**, *4*, 1349–1353.

10. Hammond, P. T. Form and Function in Multilayer Assembly: New Applications at the Nanoscale. *Adv. Mater.* **2004**, *16*, 1271–1293.

11. Tang, Z.; Wang, Y.; Podsiadlo, P.; Kotov, N. A. Biomedical Applications of Layer-by-Layer Assembly: From Biomimetics to Tissue Engineering. *Adv. Mater.* **2006**, *18*, 3203–3224.

12. Izquierdo, A.; Ono, S. S.; Voegel, J. C.; Schaaf, P.; Decher, G. Dipping *versus* Spraying: Exploring the Deposition Conditions for Speeding Up Layer-by-Layer Assembly. *Langmuir* **2005**, *21*, 7558–7567.

13. Cho, J.; Char, K.; Hong, J. D.; Lee, K. B. Fabrication of Highly Ordered Multilayer Films Using a Spin Self-Assembly Method. *Adv. Mater.* **2001**, *13*, 1076–1078.

14. Chiarelli, P. A.; Johal, M. S.; Casson, J. L.; Roberts, J. B.; Robinson, J. M.; Wang, H. L. Controlled Fabrication of Polyelectrolyte Multilayer Thin Films Using Spin-Assembly. *Adv. Mater.* **2001**, *13*, 1167–1171.

15. Shim, B. S.; Podsiadlo, P.; Lilly, D. G.; Agarwal, A.; Lee, J.; Tang, Z.; Ho, S.; Ingle, P.; Paterson, D.; Lu, W. Nanostructured Thin Films Made by Dewetting Method of Layer-By-Layer Assembly. *Nano Lett.* **2007**, *7*, 3266–3273.

16. Picart, C.; Mutterer, J.; Richert, L.; Luo, Y.; Prestwich, G. D.; Schaaf, P.; Voegel, J. C.; Lavalle, P. Molecular Basis for the Explanation of the Exponential Growth of Polyelectrolyte Multilayers. *Proc. Natl. Acad. Sci. U.S.A.* **2002**, *99*, 12531–12535.

17. Gao, H.; Ji, B.; Jager, I. L.; Arzt, E.; Fratzl, P. Materials Become Insensitive to Flaws at Nanoscale: Lessons from Nature. *Proc. Natl. Acad. Sci. U.S.A.* **2003**, *100*, 5597–5600.

18. Kamat, S.; Su, X.; Ballarin, R.; Heuer, A. H. Structural Basis for the Fracture Toughness of the Shell of the Conch *Strombus gigas*. *Nature* **2000**, *405*, 1036–1040.

19. Tesch, W.; Eidelman, N.; Roschger, P.; Goldenberg, F.; Klaushofer, K.; Fratzl, P. Graded Microstructure and Mechanical Properties of Human Crown Dentin. *Calcified Tissue Int.* **2001**, *69*, 147–157.

20. Rho, J. Y.; Kuhn-Spearing, L.; Zioupos, P. Mechanical Properties and the Hierarchical Structure of Bone. *Med. Eng. Phys.* **1998**, *20*, 92–102.

21. van Beek, J. D.; Hess, S.; Vollrath, F.; Meier, B. H. The Molecular Structure of Spider Dragline Silk: Folding and Orientation of the Protein Backbone. *Proc. Natl. Acad. Sci. U.S.A.* **2002**, *99*, 10266–10271.

22. Miserez, A.; Schneberk, T.; Sun, C.; Zok, F. W.; Waite, J. H. The Transition from Stiff to Compliant Materials in Squid Beaks. *Science* **2008**, *319*, 1816–1819.

23. Nam, S. Y.; Lee, Y. M. Pervaporation and Properties of Chitosan−Poly(acrylic acid) Complex Membranes. *J. Membr. Sci.* **1997**, *135*, 161–171.

24. Huang, Y.; Lu, J.; Xiao, C. Thermal and Mechanical Properties of Cationic Guar Gum/Poly(acrylic acid) Hydrogel Membranes. *Polym. Degrad. Stab.* **2007**, *92*, 1072–1081.

25. Gao, C.; Leporatti, S.; Moya, S.; Donath, E.; Moehwald, H. Stability and Mechanical Properties of Polyelectrolyte Capsules Obtained by Stepwise Assembly of Poly(styrenesulfonate sodium salt) and Poly(diallyldimethyl ammonium) Chloride onto Melamine Resin Particles. *Langmuir* **2001**, *17*, 3491–3495.

26. Ko, H.; Jiang, C.; Shulha, H.; Tsukruk, V. V. Carbon Nanotube Arrays Encapsulated into Freely Suspended Flexible Films. *Chem. Mater.* **2005**, *17*, 2490–2493.

27. Gunawidjaja, R.; Jiang, C.; Ko, H.; Tsukruk, V. V. Freestanding 2D Arrays of Silver Nanorods. *Adv. Mater.* **2006**, *18*, 2895–2899.

28. Al-Hussein, M.; Davies, G. R.; Ward, I. M. Mechanical Properties of Oriented Low-Density Polyethylene with an Oriented Lamellar-Stack Morphology. *J. Polym. Sci., Polym. Phys.* **2000**, *38*, 755–764.

29. Hine, P. J.; Ward, I. M. High Stiffness and High Impact Strength Polymer Composites by Hot Compaction of Oriented Fibers and Tapes. *Mechanical Properties of Polymers Based on Nanostructure and Morphology*; Taylor & Francis: Boca Raton, FL, 2005; pp 683−727.

30. Liff, S. M.; Kumar, N.; McKinley, G. H. High-Performance Elastomeric Nanocomposites via Solvent-Exchange Processing. *Nat. Mater.* **2007**, *6*, 76–83.

31. Ruokolainen, J.; Makinen, R.; Torkkeli, M.; Makela, T.; Serimaa, R.; ten Brinke, G.; Ikkala, O. Switching Supramolecular Polymeric Materials with Multiple Length Scales. *Science* **1998**, *280*, 557–560.

32. Wong, G. C. L.; Tang, J. X.; Lin, A.; Li, Y. L.; Janmey, P. A.; Safinya, C. R. Hierarchical Self-Assembly of F-Actin and Cationic Lipid Complexes: Stacked Three-Layer Tubule Networks. *Science* **2000**, *288*, 2035–2039.

33. Jenekhe, S. A.; Chen, X. L. Self-Assembly of Ordered Microporous Materials from Rod-Coil Block Copolymers. *Science* **1999**, *283*, 372–375.

34. Tang, C. B.; Lennon, E. M.; Fredrickson, G. H.; Kramer, E. J.; Hawker, C. J. Evolution of Block Copolymer Lithography to Highly Ordered Square Arrays. *Science* **2008**, *322*, 429–432.

35. Zhang, H. F.; Hussain, I.; Brust, M.; Butler, M. F.; Rannard, S. P.; Cooper, A. I. Aligned Two- and Three-Dimensional Structures by Directional Freezing of Polymers and Nanoparticles. *Nat. Mater.* **2005**, *4*, 787–793.

36. Fan, W.; Snyder, M. A.; Kumar, S.; Lee, P. S.; Yoo, W. C.; McCormick, A. V.; Penn, R. L.; Stein, A.; Tsapatsis, M. Hierarchical Nanofabrication of Microporous Crystals with Ordered Mesoporosity. *Nat. Mater.* **2008**, *7*, 984–991.

37. Yang, P. D.; Deng, T.; Zhao, D. Y.; Feng, P. Y.; Pine, D.; Chmelka, B. F.; Whitesides, G. M.; Stucky, G. D. Hierarchically Ordered Oxides. *Science* **1998**, *282*, 2244–2246.

38. Pouget, E.; Dujardin, E.; Cavalier, A.; Moreac, A.; Valery, C.; Marchi-Artzner, V.; Weiss, T.; Renault, A.; Paternostre, M.; Artzner, F. Hierarchical Architectures by Synergy between Dynamical Template Self-Assembly and Biomineralization. *Nat. Mater.* **2007**, *6*, 434–439.

39. Podsiadlo, P.; Michel, M.; Lee, J.; Verploegen, E.; Kam, N. W. S.; Ball, V.; Lee, J.; Qi, Y.; Hart, A. J; Hammond, P. T. Exponential Growth of LBL Films with Incorporated Inorganic Sheets. *Nano Lett.* **2008**, *8*, 1762–1770.

40. Masters, J. E., Ed. *Damage Detection in Composite Materials*. Papers Presented at the International Symposium on Damage Detection and Quality Assurance in Composite Materials, San Antonio, Texas, 13−14 Nov, 1990 [In: *ASTM Spec. Tech. Publ.*, 1992; STP 1128], 1992.